

# Phase Transition Behavior of Rare Earth Oxide $\text{Ce}_2\text{O}_3$ in $\text{CaO-SiO}_2-5\text{wt.}\% \text{Al}_2\text{O}_3$ System at 1673–1873 K



Rensheng Li, Renyi Yang, Xu Gao, Wanlin Wang, and You Zhou

**Abstract** Based on previous phase diagram studies on the  $\text{CaO-SiO}_2\text{-Ce}_2\text{O}_3\text{-}5\text{wt.}\% \text{Al}_2\text{O}_3$  system at 1673–1773 K. In this study, the equilibrium phase diagram experiment at 1873 K was extended. The phase composition and phase ratio were analyzed and statistically calculated by FE-SEM, XRD, EPMA, and XRF, so the equilibrium phase diagram of  $\text{CaO-SiO}_2\text{-Ce}_2\text{O}_3\text{-}5\text{wt.}\% \text{Al}_2\text{O}_3$  at 1873 K was obtained. At this high temperature, the phases coexisting with the liquid phase are  $\text{CaO}\cdot 2\text{Ce}_2\text{O}_3\cdot 3\text{SiO}_2$ ,  $\text{SiO}_2$ ,  $\text{Ca}_2\text{SiO}_4$ , and  $\text{Ce}_2\text{Si}_2\text{O}_7$ . In addition, the liquid phase region and the initial crystal point at the temperature of 1673–1873 K in  $\text{CaO-SiO}_2\text{-Ce}_2\text{O}_3\text{-}5\text{wt.}\% \text{Al}_2\text{O}_3$  system were plotted. The precipitation and phase transformation behavior of rare earth oxide  $\text{Ce}_2\text{O}_3$  in  $\text{CaO-SiO}_2\text{-Al}_2\text{O}_3$  are explained in detail, which provides a theoretical basis for the value-added utilization of rare earth oxides.

**Keywords** Rare earth · Phase equilibria · Experimental thermodynamics · Liquidus

## Introduction

The formation of rare earth-bearing phases in pyrometallurgical processes can be estimated and evaluated using the phase equilibrium of the system. The experimental measurement method of the phase diagram can be divided into dynamic method

---

R. Li · R. Yang · X. Gao · W. Wang (✉) · Y. Zhou  
School of Metallurgy and Environment, Central South University, Changsha 410083, China  
e-mail: [wanlin.wang@gmail.com](mailto:wanlin.wang@gmail.com)

R. Li  
e-mail: [rensheng.li@csu.edu.cn](mailto:rensheng.li@csu.edu.cn)

R. Yang  
e-mail: [223512089@csu.edu.cn](mailto:223512089@csu.edu.cn)

Y. Zhou  
e-mail: [zhouyou2010@csu.edu.cn](mailto:zhouyou2010@csu.edu.cn)

and the static method according to the difference in the experimental measurement principle [1]. The dynamic method is that when the components of the experimental point cross the phase boundary, the physicochemical properties of the system on the phase boundary will also change due to the change of the phase structure. Static method, also known as isothermal method, a series of samples with known component content at a specific temperature to heat treatment, so that the sample reaches a stable equilibrium state. The representative method of the static method is the quenching method, also known as the high temperature equilibrium experimental method [2]. The research method used in this study is the high temperature equilibrium method.

Recently, with the development of science and technology and the maturity of the application of detection methods, many scholars have carried out more and more research on rare earth-containing oxide systems, which greatly enriched and supplemented the basic information of relevant thermodynamics. In order to understand the role of  $\text{Ce}_2\text{O}_3$  in sulfur dissolution behavior, Jeong et al. [3] determined the sulfide capacity of  $\text{MnO-SiO}_2\text{-Al}_2\text{O}_3\text{-Ce}_2\text{O}_3$  system at  $1600^\circ\text{C}$  by gas-residue equilibrium method, and analyzed its structure by Raman microscopy. Tas et. al [4, 5] conducted a systematic study on the thermodynamic behavior of  $\text{Ce}_2\text{O}_3\text{-Ce}_2\text{Si}_2\text{O}_7$  system from  $1150^\circ\text{C}$  to  $1970^\circ\text{C}$ , and found that a total of three eutectic reactions occurred in the system at  $1664^\circ\text{C} \pm 5^\circ\text{C}$ ,  $1870^\circ\text{C} \pm 25^\circ\text{C}$ ,  $1762^\circ\text{C} \pm 10^\circ\text{C}$ , and a relatively complete phase diagram of the  $\text{Ce}_2\text{O}_3\text{-Ce}_2\text{Si}_2\text{O}_7$  system was measured for the first time.

In the production of rare earth ceramics, rare earth glass, rare earth steel, and other related materials,  $\text{CaO-SiO}_2\text{-RE}_2\text{O}_3$  system is the basic slag system, and the phase transition is the necessary thermodynamic basis for practical applications. There are many studies on the role and advantages of rare earths in material applications, but there are few studies on rare earth oxide phase diagrams, and only some binary phase diagrams have been completely constructed. However, the thermodynamic property of complex systems involved in practical applications of rare earths cannot be obtained from these simple binary systems, but there are very few studies containing rare earth elements, such as  $\text{CaO-SiO}_2\text{-Ce}_2\text{O}_3$  [6]. Qiu et al. conducted a large number of experimental studies on  $\text{La}_2\text{O}_3$ -containing systems [7–13], and determined the existence of the solid solution phase of the ternary compound  $\text{CaO}\cdot 3\text{SiO}_2\cdot 2\text{La}_2\text{O}_3$ , and obtained the isothermal cross-sectional diagram of  $\text{CaO-SiO}_2\text{-Nb}_2\text{O}_5\text{-La}_2\text{O}_3$  ternary system at specific temperature, which enriched the thermodynamic data of  $\text{La}_2\text{O}_3$ -containing system. Lan et al. [14–16] presented the thermodynamic data of  $\text{CaO-SiO}_2\text{-Ce}_2\text{O}_3$  ternary system,  $\text{CaO-SiO}_2\text{-CaF}_2\text{-Ce}_2\text{O}_3$  quaternary system, and  $\text{CaO-SiO}_2\text{-CaF}_2\text{-P}_2\text{O}_5\text{-Ce}_2\text{O}_3$  quinary system at specific temperatures, and studied the crystallization behavior of REE phase ( $\text{Ce}_{9.33-x}\text{Ca}_x(\text{SiO}_4)_6\text{O}_{2.0.5x}$ ). The temperature range of REE phase crystallization separately in REE-containing slag of selected components, as well as the crystallization and growth kinetics of cerium fluorosilica ( $\text{Ce}_{9.33-x}\text{Ca}_x(\text{SiO}_4)_4\text{O}_{5.0.5x}\text{F}_2$ ) and the formation mechanism of cerium apatite ( $\text{Ca}_{5-x}\text{Ce}_x[(\text{Si}, \text{P})\text{O}_4]_3\text{F}$ ) were obtained, which provided a theoretical basis for the sustainable utilization of rare earth elements in rare earth slag in ceramics and rare earth resource recovery. On this basis, the equilibrium phase composition

of SiO<sub>2</sub>-Ce<sub>2</sub>O<sub>3</sub>-CaO-5wt.% Al<sub>2</sub>O<sub>3</sub> at 1673–1873 K was studied in this paper, which provided basic phase transition data for the recycling of rare earth waste residue in ceramics and other fields.

## Methodology

### *Rare Earth Slag Samples Preparation*

To ensure the accuracy of the experimental results, all the experimental slag samples were pre-melted. In the pre-melting test, an electronic balance with an accuracy of 0.0001 g was used to weigh the required oxide powder according to the design composition and mix evenly. Then, A platinum crucible was used to contain the oxide mixture powder and placed in the constant temperature zone of a high-frequency induction heating furnace. The temperature was raised to 1923 K for 4 h under the atmosphere of Ar + 10% H<sub>2</sub> to obtain a liquid phase slag with uniform composition. After the pre-melting time was finished, the slag sample was quickly put into the ice-water mixture and quenched.

In order to confirm whether the pre-slag is a uniform glass phase due to the crystal precipitation easy occur during the quenching process. It is necessary to test whether the pre-slag is a uniform glass phase. The pre-slag was ground in an agate mortar, and part of the sample was taken for XRD detection (X-ray Diffraction, Empyrean 2, PANalytical), and Fig. 1 shows the micromorphology and XRD detection pattern of the homogeneous glass phase of N1 sample. In addition, it is also necessary to detect the valence state of Ce in the pre-slag sample, because this study mainly investigates the equilibrium phase of Ce with Ce<sub>2</sub>O<sub>3</sub> when it is stable in the cerium-containing slag system. Therefore, the remaining slag sample after grinding was detected by XPS (X-ray Photoelectron Spectroscopy, ESCALAB250Xi, ThermoScientific). For instance, the XPS spectrum of 3d<sub>5/2</sub> and 3d<sub>3/2</sub> of Ce<sup>3+</sup> ions of N1 sample are shown in Fig. 2. Due to the transition behavior between the two different energy levels of Ce<sup>3+</sup> ions, the emergence of 3d<sub>5/2</sub> and 3d<sub>3/2</sub> was found in Fig. 2. This result indicates that only Ce<sup>3+</sup> is present and not Ce<sup>4+</sup> in the pre-melted sample. For slag samples with XRD detection determined to be glass phase and XPS detection determined that the valence state of Ce is completely + 3 valence, the XRF instrument (X-ray Fluorescence Spectrometer, AxiosmAX, PANalytical) was used to determine the pre-slag composition.

Due to the burning loss and weighing error of the test, the composition of the pre-melted slag may be different from the design. Therefore, it is necessary to detect the composition of quenching slag. The XRF was used to analyze the composition of the pre-melted slag samples, and the results are listed in Table 1. It can be found that there is only a slight deviation in the measured value compared to the design

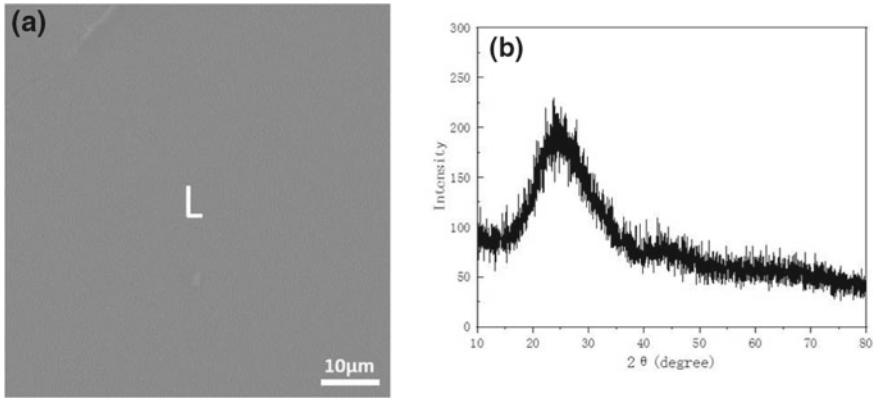


Fig. 1 Microstructure **a** and XRD patterns **b** of pre-melted slag sample N1

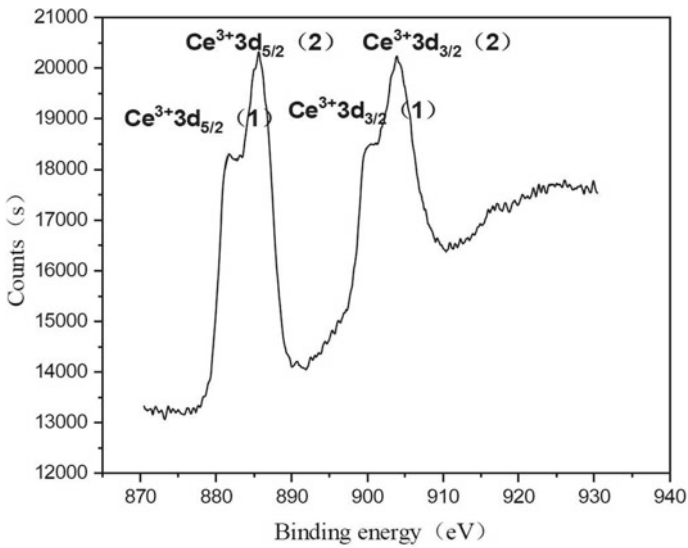


Fig. 2 XPS detection map of quenching slag sample N1

component. In order to more intuitively see the composition distribution of the pre-melted slag sample, the detection point is placed in the pseudo-ternary phase diagram of the  $SiO_2-Ce_2O_3-CaO-5wt.\% Al_2O_3$  system, as shown in Fig. 3.

**Table 1** Comparison of design and tested composition of samples for CaO-SiO<sub>2</sub>-Ce<sub>2</sub>O<sub>3</sub>-5wt.% Al<sub>2</sub>O<sub>3</sub>

Sample		Al <sub>2</sub> O <sub>3</sub>	SiO <sub>2</sub>	Ce <sub>2</sub> O <sub>3</sub>	CaO	Sum
N5	Designed	5	38	28.5	28.5	100
	Measured	4.98	38.21	28.64	28.17	100
N6	Designed	5	35	55	5	100
	Measured	5.29	35.38	54.01	5.32	100
N7	Designed	5	38	33.25	23.75	100
	Measured	4.89	38.4	33.21	23.5	100
N8	Designed	5	38	42.75	14.25	100
	Measured	5.04	32.53	43.95	18.48	100
N11	Designed	5	76	4.75	14.25	100
	Measured	5.09	77.96	4.32	12.63	100
N14	Designed	5	66.5	16.625	11.875	100
	Measured	4.95	68.27	16.08	10.70	100
N16	Designed	5	66.5	23.75	4.75	100
	Measured	4.64	67.09	23.68	4.59	100
N17	Designed	5	38	22.8	34.2	100
	Measured	4.83	38.7	24.01	32.46	100
N19	Designed	5	36.1	29.45	29.45	100
	Measured	5.44	38.69	17.89	38.43	100
N20	Designed	5	52.25	28.5	14.25	100
	Measured	4.99	50.2	29.6	14.76	100
N25	Designed	5	67.45	0	27.55	100
	Measured	4.97	69.16	0	25.87	100
N26	Designed	5	39.9	2.85	52.25	100
	Measured	5.23	40.54	12.36	41.87	100
N29	Designed	5	39.9	7.6	47.5	100
	Measured	5.27	41.63	9.28	43.82	100
N31	Designed	5	39	56	0	100
	Measured	5.31	38.28	56.41	0	100
N32	Designed	5	73	22	0	100
	Measured	5.47	72.50	22.03	0	100

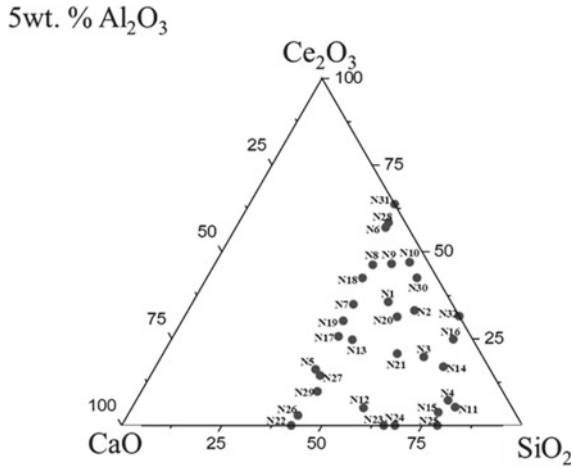


Fig. 3 Pre-melting component points of SiO<sub>2</sub>-Ce<sub>2</sub>O<sub>3</sub>-CaO-5wt. % Al<sub>2</sub>O<sub>3</sub> system at 1673–1873 K

### Equilibration Experiments

The chamber furnace was used to perform a phase equilibrium experiment at high temperature, as shown in Fig. 4a. The experimental temperature is measured by a type B thermocouple placed at the bottom of the furnace. Temperature control accuracy up to ± 1 K. In addition, the equilibrium time, experimental atmosphere, and quenching method are the main factors affecting the accuracy of high temperature equilibrium experimental results. Therefore, the atmosphere in the experiment consists of 10% H<sub>2</sub> in high-purity Ar and purified by a gas purification device, as shown in Fig. 4b.

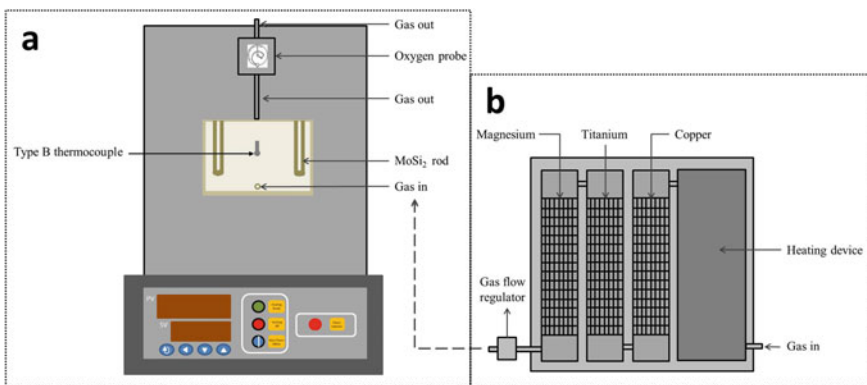


Fig. 4 Schematic diagram of a box-type furnace and b gas purification unit

To ensure that the slag sample is not oxidized and to isolate other possible sources of contamination. The deaeration unit was composed of heating device and copper, sponge titanium, and magnesium deaeration chamber, which can keep the partial pressure of oxygen in argon below  $10^{-16}$ . In the experiment, about 2 g of homogenized glass phase slag sample was weighed into a platinum crucible and placed in the constant temperature zone of the chamber furnace. All samples are heated again to 1923 K and held warm for 30 min, then cooled at a faster rate (10 K/min) to the target equilibrium temperature (1873 K). Based on the previous experimental results and the experimental experience of predecessors [17], the equilibrium time was set at 24 h.

After the equilibrium time was reached, the sample was quickly placed into the ice-water mixture for quenching. The quenched sample was then dried at 120 °C. Electron Probe Microanalysis (EPMA, JXA-8230) was employed to perform compositional analysis of each sample and XRD was used to detect the precipitated phase contained in the slag sample. In addition, the coexistence phase was observed using a Scanning Electron Microscope (SEM, JSM-7900F). The equilibrium micromorphology of the sample was obtained in BSE mode. The SEM test conditions: the beam current is 13 mA, the accelerating voltage is 20 kV. The EPMA measurement conditions: the beam current is  $10^{-8}$  A, the accelerating voltage is 20 kV and the probe diameter is 1 μm. The CaSiO<sub>3</sub>, Al<sub>2</sub>O<sub>3</sub>, and CeP<sub>5</sub>O<sub>14</sub> were used as the standard to analyze CaO, SiO<sub>2</sub>, Al<sub>2</sub>O<sub>3</sub>, and Ce<sub>2</sub>O<sub>3</sub>, respectively. For each equilibrium phase, more than 10 different points were analyzed and averages calculated. Combined with the test results of XRD, FE-SEM, and EPMA, the phase composition of the sample in equilibrium was obtained.

## Results and Discussion

### *Equilibrium Phase Composition of SiO<sub>2</sub>-Ce<sub>2</sub>O<sub>3</sub>-CaO-5wt.% Al<sub>2</sub>O<sub>3</sub> System at 1873 K*

Since the phase equilibrium results of CaO-SiO<sub>2</sub>-Ce<sub>2</sub>O<sub>3</sub>-5wt.% Al<sub>2</sub>O<sub>3</sub> system at 1673–1773 K have been studied in the previous work [17], this part only shows the phase equilibrium results at 1873 K. When the temperature of CaO-SiO<sub>2</sub>-Ce<sub>2</sub>O<sub>3</sub>-5wt.% Al<sub>2</sub>O<sub>3</sub> system increased to 1873 K, the phase equilibrium relationship became simpler, most of the samples were displayed as pure liquid phase after 24 h of equilibrium, only a few samples appeared precipitated phase, and the microscopic morphology of the precipitated phase did not change much, as shown in Fig. 5.

Figure 5 shows the micromorphology of sample N14 and XRD test results, it can be seen that SiO<sub>2</sub> with black rod and dot equilibrium phase coexists with liquid phase in the gray area (Fig. 5a), and the samples N11, N16, N25, and N32 are the same. When

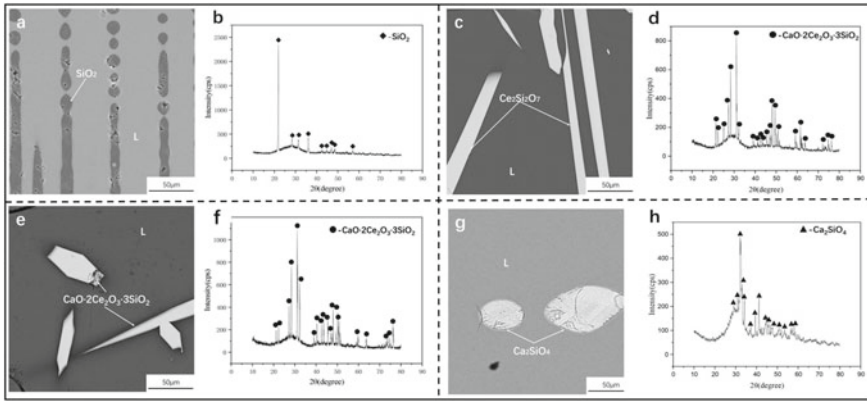


**Fig. 5** Microstructure of the equilibrium phase of the CaO-SiO<sub>2</sub>-Ce<sub>2</sub>O<sub>3</sub>-5wt.%Al<sub>2</sub>O<sub>3</sub> system at 1873 K and the corresponding XRD detection patterns (a Microstructure of sample N14, b XRD detection pattern of sample N14, c Microstructure of sample N31, d XRD detection pattern of sample N31, e Microstructure of sample N7, f XRD pattern of sample N7, g Microstructure of sample N26, and h XRD pattern of sample N26)

the sample components are adjusted to the same as N31, the micromorphology of the high temperature equilibrium phase is shown in Fig. 5c, combined with the XRD test results, it can be found that the gray-white sword-like is the Ce<sub>2</sub>Si<sub>2</sub>O<sub>7</sub> phase, and the EPMA detection results show that Ca<sup>2+</sup> does not replace Ce<sup>3+</sup> in Ce<sub>2</sub>Si<sub>2</sub>O<sub>7</sub>. In samples N5–N8, N17, and N19, a regular hexagonal CaO·2Ce<sub>2</sub>O<sub>3</sub>·3SiO<sub>2</sub> was detected, and its microscopic morphology is shown in Fig. 5e. The EPMA test results shows that there were both Ca elements and Ce elements in the precipitated phases of N26 and N29, and their microscopic morphology is shown in Fig. 5g, combined with the XRD test results, it could be judged that the gray-white dots were (Ca, Ce)<sub>2</sub>SiO<sub>4</sub> phase. Table 2 lists the composition of all phases in each sample under investigation, similarly, in samples with ‘\*’, the precipitated phase Ca<sub>2</sub>SiO<sub>4</sub> is obtained by converting Ce<sup>3+</sup> to Ca<sup>2+</sup>. All measured compositional data are normalized and used to construct phase diagrams.

### ***Determination of the Isotherms at 1673–1873 K***

During the preparation of the sample, the content of Al<sub>2</sub>O<sub>3</sub> was set to 5 wt.%. However, due to the crystal precipitation in the slag, the Al<sub>2</sub>O<sub>3</sub> content in the quenched liquid phase cannot be accurate at 5 wt.%. Therefore, the liquid composition after quenching must be standardized in order to use the phase diagram to represent the phase relationship of CaO-SiO<sub>2</sub>-Ce<sub>2</sub>O<sub>3</sub>-5wt.% Al<sub>2</sub>O<sub>3</sub> system [18, 19]. As shown in Fig. 6, the liquid phase isotherms of SiO<sub>2</sub>-Ce<sub>2</sub>O<sub>3</sub>-CaO-5wt.% Al<sub>2</sub>O<sub>3</sub> system at 1673–1873 K are obtained based on the above experimental results.



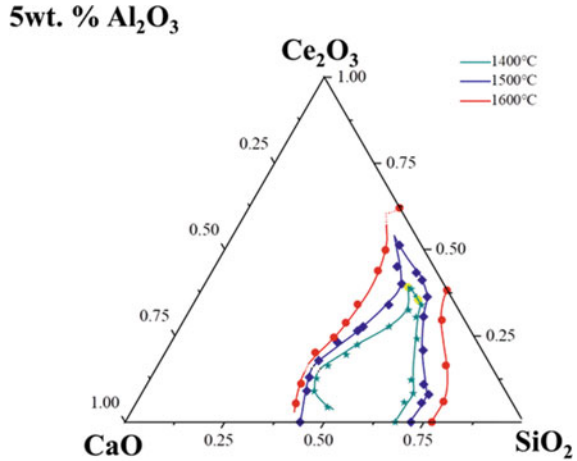
**Table 2** Equilibrium phase composition of the CaO-SiO<sub>2</sub>-Ce<sub>2</sub>O<sub>3</sub>-5wt.%Al<sub>2</sub>O<sub>3</sub> system at 1600 °C

Sample	Phase	Components(wt.%)				Sum
		Al <sub>2</sub> O <sub>3</sub>	SiO <sub>2</sub>	Ce <sub>2</sub> O <sub>3</sub>	CaO	
N5	L	5.67	35.54	19.01	39.78	100
	CaO·2Ce <sub>2</sub> O <sub>3</sub> ·3SiO <sub>2</sub>	0.05	20.48	72.69	6.78	100
N6	L	5.58	38.17	47.06	9.19	100
	CaO·2Ce <sub>2</sub> O <sub>3</sub> ·3SiO <sub>2</sub>	0.03	20.63	72.64	6.7	100
N7	L	4.65	39.37	32.56	23.42	100
	CaO·2Ce <sub>2</sub> O <sub>3</sub> ·3SiO <sub>2</sub>	0.02	20.62	72.59	6.77	100
N8	L	5.53	39.23	41.46	13.78	100
	CaO·2Ce <sub>2</sub> O <sub>3</sub> ·3SiO <sub>2</sub>	0.02	20.57	72.81	6.60	100
N11	L	5.2	72.94	5.65	16.21	100
	SiO <sub>2</sub>	0.44	98.73	0.44	0.39	100
N14	L	5.56	68.28	15.52	10.64	100
	SiO <sub>2</sub>	0.45	98.71	0.52	0.32	100
N16	L	5.85	60.93	27.84	5.38	100
	SiO <sub>2</sub>	0.18	99.12	0.24	0.46	100
N17	L	5.81	37.82	23.11	33.26	100
	CaO·2Ce <sub>2</sub> O <sub>3</sub> ·3SiO <sub>2</sub>	0.18	21.69	70.82	7.31	100
N19	L	5.94	38.54	27.11	28.41	100
	CaO·2Ce <sub>2</sub> O <sub>3</sub> ·3SiO <sub>2</sub>	0.16	21.13	72.73	5.98	100
N25	L	5.74	72.58	0	21.68	100
	SiO <sub>2</sub>	0.24	99.35	0.23	0.18	100
N26*	L	4.98	38.17	5.15	51.7	100
	Ca <sub>2</sub> SiO <sub>4</sub>	0.33	31.54	15.01	53.12	100
N29*	L	5.48	36.5	10.52	47.5	100
	Ca <sub>2</sub> SiO <sub>4</sub>	0.36	31.65	17.9	50.09	100
N31	L	5.16	35.89	58.87	0.08	100
	Ce <sub>2</sub> Si <sub>2</sub> O <sub>7</sub>	0.09	25.01	74.82	0.08	100
N32	L	6.99	57.37	35.55	0.09	100
	SiO <sub>2</sub>	0.41	98.1	0.45	1.04	100

\* Represents the results that Ce<sup>3+</sup> have been converted to Ca<sup>2+</sup>

It can be seen that when the content of Al<sub>2</sub>O<sub>3</sub> is constant at 5%, with the increase of temperature, the liquid line moves closer to the Ce<sub>2</sub>O<sub>3</sub>-SiO<sub>2</sub> boundary line. When the temperature reaches 1873 K, a large liquid region appears on the Ce<sub>2</sub>O<sub>3</sub>-SiO<sub>2</sub> boundary line. In addition, when the temperature is 1673 K, it is necessary to add at least 13 wt.% CaO to form the liquid phase region. When the temperature rises to 1773 K, it is necessary to add at least 8 wt.% CaO to form the liquid phase region. When the temperature rises to 1873 K, it is only necessary to adjust the ratio of SiO<sub>2</sub>/

**Fig. 6** Liquid phase isotherms of  $\text{SiO}_2\text{-Ce}_2\text{O}_3\text{-CaO-5wt.}\%$   $\text{Al}_2\text{O}_3$  system at 1673–1873 K



$\text{Ce}_2\text{O}_3$  to form the liquid phase region. It shows that in the  $\text{SiO}_2\text{-Ce}_2\text{O}_3\text{-5wt.}\%$   $\text{Al}_2\text{O}_3$  system, when the ratio of  $\text{SiO}_2/\text{Ce}_2\text{O}_3$  is moderate, the addition of an appropriate amount of CaO can significantly reduce the melting point of the mixed oxide. This also provides a new idea for solving the problem of nozzle clogging caused by  $\text{Ce}_2\text{O}_3$ -type high-melting-point fine inclusions produced in the smelting process of rare earth steel, that is, the high-melting-point rare earth enrichment phase can be modified into a low-melting-point phase through the synergistic effect of calcium-silicon or calcium-aluminum, so as to fundamentally solve the clogging problem caused by the enrichment of high-melting-point fine inclusions at the nozzle, which is also a focus of our subsequent research.

In the above research system, the basicity range in the liquid phase region increases with the decrease of  $\text{Ce}_2\text{O}_3$  content. At a fixed basicity, the liquidus temperature increases with the increase of  $\text{Ce}_2\text{O}_3$  content. At the same time, obvious knob phenomenon was observed on each isotherm, and the composition of knob moved to higher basicity and higher  $\text{Ce}_2\text{O}_3$  content with the increase of temperature.

### ***Construction of $\text{SiO}_2\text{-Ce}_2\text{O}_3\text{-CaO-5wt.}\%$ $\text{Al}_2\text{O}_3$ System Phase Diagram***

Phase diagram can be used to quantitatively describe the phase equilibrium of systems. It can help to determine the direction of a reaction and avoid the resource consumption during the research process. Combining the isotherms of  $\text{SiO}_2\text{-Ce}_2\text{O}_3\text{-CaO-5wt.}\%$   $\text{Al}_2\text{O}_3$  system at 1673–1873 K with the above equilibrium phase structure, a phase diagram related to the system containing rare earth was constructed, as shown in Fig. 7. According to the trend of phase boundary, the intersection point of

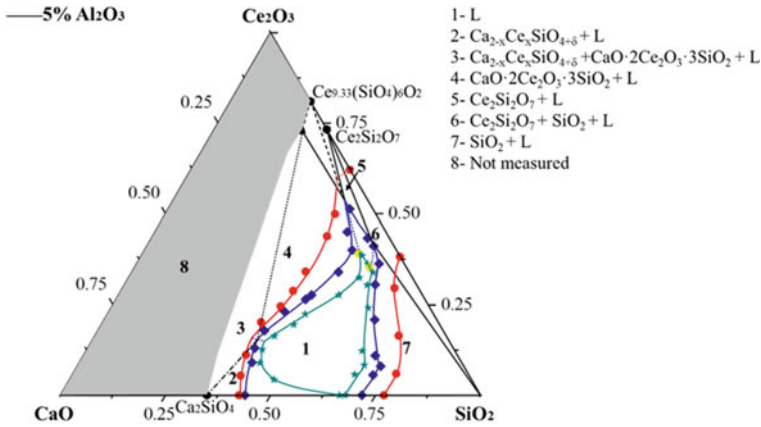


Fig. 7 Phase diagram of SiO<sub>2</sub>-Ce<sub>2</sub>O<sub>3</sub>-CaO-5wt.% Al<sub>2</sub>O<sub>3</sub> system

phase boundary is found. Meanwhile, several points on the CaO-SiO<sub>2</sub> phase boundary are data points obtained according to the known phase diagram [20].

Combining the current results with the phase diagram information of CaO-SiO<sub>2</sub>-Ce<sub>2</sub>O<sub>3</sub> [6], the isotherms and phase relationships of specific compositions related to rare earth element Ce were constructed in Fig. 7. It is worth noting that the liquid phase data points on the SiO<sub>2</sub>-CaO line, that is, when the content of Ce<sub>2</sub>O<sub>3</sub> is 0, the data obtained by the experiment in this study are basically consistent with the known CaO-SiO<sub>2</sub>-Al<sub>2</sub>O<sub>3</sub> system phase diagram [20] data points, which again proves that the experiment has high accuracy. In the region from 1 to 6, according to the law of the adjacent phase region and the trend of the phase boundary line shown by the experimental results, the phase relationship between region 2 and region 3, region 3 and region 4 is deduced, that is, the three-phase equilibrium between Ca<sub>2-x</sub>Ce<sub>x</sub>SiO<sub>4+x</sub>, CaO·2Ce<sub>2</sub>O<sub>3</sub>·3SiO<sub>2</sub> and liquid phase, and the two-phase equilibrium between Ce<sub>2</sub>Si<sub>2</sub>O<sub>7</sub> and liquid phase. In addition, the phase relationship in the solid phase region with SiO<sub>2</sub> content less than 20 wt.% and the dotted region is not studied in this work.

The equilibrium state detected from 1673 K and the change trend of the primary crystal phase at 1773 K can be summarized as follows. The liquid phase region is mainly in the range of SiO<sub>2</sub> content in 50 wt.%-75 wt.%. In the low Ce<sub>2</sub>O<sub>3</sub> content and low basicity region, the primary phase is SiO<sub>2</sub>. In the region of high basicity and low Ce<sub>2</sub>O<sub>3</sub> content, the precipitated phase is Ca<sub>2</sub>SiO<sub>4</sub>. With the increase of Ce<sub>2</sub>O<sub>3</sub> content, the main precipitated phase is transformed into CaO·2Ce<sub>2</sub>O<sub>3</sub>·3SiO<sub>2</sub>. It can be found that the liquidus at 1673 K is very close to the liquidus at 1773 K in the large area near the phase boundary between Ca<sub>2-x</sub>Ce<sub>x</sub>SiO<sub>4+x</sub> and CaO·2Ce<sub>2</sub>O<sub>3</sub>·3SiO<sub>2</sub>. This indicates that the area of the primary crystal zone of CaO·2Ce<sub>2</sub>O<sub>3</sub>·3SiO<sub>2</sub> in the system of this study is less affected by temperature in the range of 1673 K to 1773 K, and is greatly affected by basicity.

## Conclusions

In the current study, the phase equilibrium relationship of CaO-SiO<sub>2</sub>-Ce<sub>2</sub>O<sub>3</sub>-5wt.% Al<sub>2</sub>O<sub>3</sub> phase diagram system was studied. By using XRD, XRF, EPMA, FE-SEM, and EDS analysis, the equilibrium phase at 1673–1873 K was determined. The main results can be summarized as follows:

- (1) The compositions of liquid phase (L), CaO·2Ce<sub>2</sub>O<sub>3</sub>·3SiO<sub>2</sub> solid solution phase, Ca<sub>2-x</sub>Ce<sub>x</sub>SiO<sub>4</sub> + δ (Ca<sub>2</sub>SiO<sub>4</sub>, as shown in Fig. 9, by converting Ce<sup>3+</sup> to Ca<sup>2+</sup>) solid solution phase and Ce<sub>2</sub>Si<sub>2</sub>O<sub>7</sub> phase were determined by high temperature equilibrium technique at 1673–1873 K.
- (2) The isothermal liquid phase of CaO-SiO<sub>2</sub>-Ce<sub>2</sub>O<sub>3</sub>-5wt.% Al<sub>2</sub>O<sub>3</sub> system at 1673–1873 K was determined by high temperature equilibrium experiment. At the same time, the location of the primary crystal zone of the four precipitated phases was determined.
- (3) According to the experimental results, the isothermal section diagram of CaO-SiO<sub>2</sub>-Ce<sub>2</sub>O<sub>3</sub>-5wt.% Al<sub>2</sub>O<sub>3</sub> system at 1673–1873 K was obtained.

## References

1. Zhao J (2007) Methods for phase diagram determination. Elsevier Sci, USA
2. Wang P, Xu Q (2005) Materials research method (Chinese version). Sci press, Beijing
3. Jeong S, Kim T, Park J (2017) Relationship between sulfide capacity and structure of MnO-SiO<sub>2</sub>-Al<sub>2</sub>O<sub>3</sub>-Ce<sub>2</sub>O<sub>3</sub> system. Metall Mater Trans B 48(1):545–553
4. Tas A, Akinc M (1994) Phase relations in the system Ce<sub>2</sub>O<sub>3</sub>-Ce<sub>2</sub>Si<sub>2</sub>O<sub>7</sub> in the temperature range 1150° to 1970°C in reducing and inert atmospheres. J Am Ceram Soc 77(11):2953–2960
5. Tas A, Akinc M (1994) Phase relations in the system Ce<sub>2</sub>O<sub>3</sub>-Al<sub>2</sub>O<sub>3</sub> in inert and reducing atmospheres. J Am Ceram Soc 77(11):2961–2967
6. Zhao Z, Chen X, Yan GB, B, (2019) Experimental study on the thermodynamics of the CaO-SiO<sub>2</sub>-Ce<sub>2</sub>O<sub>3</sub> system at 1873 K. Metall Mater Trans B 50(1):395–406
7. Qiu J, Liu C, Yu Z (2018) Isothermal section of CaO-SiO<sub>2</sub>-La<sub>2</sub>O<sub>3</sub> system within specific region at 1673–1473 K. Ceram Int 44(11):12564–12572
8. Qiu J, Liu C, Liu Z, Yu Z (2019) Phase equilibria in medium basicity region of CaO-SiO<sub>2</sub>-Nb<sub>2</sub>O<sub>5</sub>-(5%, 10%, 15%) La<sub>2</sub>O<sub>3</sub> system. Ceram Int 45(2, Part A):2281–2288
9. Liu C, Qiu J (2018) Phase equilibrium relations in the specific region of CaO-SiO<sub>2</sub>-La<sub>2</sub>O<sub>3</sub> system. J Eur Ceram Soc 38(4):2090–2097
10. Qiu J, Liu C (2017) Subsolidus phase relations in the CaO-SiO<sub>2</sub>-Nb<sub>2</sub>O<sub>5</sub>-La<sub>2</sub>O<sub>3</sub> quaternary system at 1273 K. ISIJ Int 57(12):2107–2114
11. Liu C, Qiu J, Sun L (2018) Liquidus and phase equilibrium in CaO-SiO<sub>2</sub>-Nb<sub>2</sub>O<sub>5</sub>-10%La<sub>2</sub>O<sub>3</sub> system. ISIJ Int 58(4):612–619
12. Qiu J, Liu C, Liu Z, Yu Z (2020) Phase equilibria in low basicity region of CaO-SiO<sub>2</sub>-Nb<sub>2</sub>O<sub>5</sub>-(5 wt%, 10 wt%, 15 wt%) La<sub>2</sub>O<sub>3</sub> system. J Rare Earths 38(1):100–107
13. Qiu J, Liu C (2017) Solid phase equilibrium relations in the CaO-SiO<sub>2</sub>-Nb<sub>2</sub>O<sub>5</sub>-La<sub>2</sub>O<sub>3</sub> system at 1273 K. Metall Mater Trans B 49(1):69–77
14. Lan X, Gao J, Du Y, Guo Z (2020) Thermodynamics and crystallization kinetics of REEs in CaO-SiO<sub>2</sub>-Ce<sub>2</sub>O<sub>3</sub> system. J Am Ceram Soc 103(4):2845–2858

15. Lan X, Gao J, Li Y, Guo Z (2021) Thermodynamics and kinetics of REEs in  $\text{CaO-SiO}_2\text{-CaF}_2\text{-Ce}_2\text{O}_3$  system: A theoretical basis toward sustainable utilization of REEs in REE-bearing slag. *Ceram Int* 47(5):6130–6138
16. Lan X, Gao J, Li Y, Guo Z (2021) Phase equilibria of  $\text{CaO-SiO}_2\text{-CaF}_2\text{-P}_2\text{O}_5\text{-Ce}_2\text{O}_3$  system and formation mechanism of britholite. *Ceram Int* 47(9):11966–11972
17. Zhang T, Li M, Li R, Wang W (2022) Phase Equilibria and thermodynamic properties of low basicity RE-contained slags by critical evaluation and experiment. *Metall Mater Trans B* 53(5):3044–3053
18. Wang Z, Sun H, Zhang L, Zhu Q (2016) Phase equilibria in the  $\text{TiO}_2$  rich part of the  $\text{TiO}_2\text{-CaO-SiO}_2\text{-10wt.\%Al}_2\text{O}_3$  system at 1773 K and 1873 K. *J Alloys Compd* 671:137–143
19. Gran J, Wang Y, Sichen D (2011) Experimental determination of the liquidus in the high basicity region in the  $\text{Al}_2\text{O}_3(30 \text{ mass\%})\text{-CaO-MgO-SiO}_2$  system. *Calphad* 35(2):249–254
20. Eisenhüttenleute VD (1995) *SLAG ATLAS*, 2nd edn. Verlag stahleisen GmbH, Germany